International Journal of Nanomedicine

Dovepress
Taylor & Francis Group

Open Access Full Text Article

ORIGINAL RESEARCH

MXene-Mediated Nanocarrier Delivery Enhances the Chondroprotective Effects of Quercetin in Experimental Osteoarthritis

Kaifeng Gan[1–3,*], Jie Li[1–3,*], Xuyang Zhang[2,3], Zhenhua Feng[2,3], Junhui Liu[2,3], Fengdong Zhao[2,3]

[1]Department of Orthopaedic Surgery, the Affiliated LiHuiLi Hospital of Ningbo University, Ningbo, Zhejiang, 315040, People's Republic of China; [2]Department of Orthopaedic Surgery, Sir Run Run Shaw Hospital, Zhejiang University School of Medicine, Hangzhou, Zhejiang, 310016, People's Republic of China; [3]Zhejiang Key Laboratory of Mechanism Research and Precision Repair of Orthopaedic Trauma and Aging Diseases, Hangzhou, Zhejiang, 310016, People's Republic of China

*These authors contributed equally to this work

Correspondence: Fengdong Zhao, Department of Orthopaedic Surgery, Sir Run Run Shaw Hospital, Zhejiang University School of Medicine, Hangzhou, Zhejiang, 310016, People's Republic of China, Email zhaofengdong@zju.edu.cn

Introduction: Osteoarthritis (OA) is a common chronic joint disease that severely affects patients' quality of life. Quercetin, a natural flavonoid, exhibits chondroprotective effects, though its bioavailability through regular oral consumption is limited. In this study, we employed two-dimensional MXene nanosheets as a nanocarrier to facilitate targeted intracellular delivery of quercetin, aiming to enhance its therapeutic efficacy against OA.

Methods: Methods: Porous $Ti_3C_2T_x$ MXene nanosheets were synthesized via selective etching and then loaded with quercetin through physical adsorption. Material characterization was performed using transmission electron microscopy (TEM), scanning electron microscopy (SEM), ultraviolet–visible spectroscopy (UV–Vis), dynamic light scattering (DLS), and in vitro release assays. For in vitro evaluation, IL-1β-stimulated primary mouse articular chondrocytes (ACs) were treated with free quercetin or MXene-loaded quercetin, followed by assessments of cell viability, apoptosis, cell cycle progression, migration, oxidative stress markers, and ferroptosis-related protein expression. For in vivo validation, a destabilization of the medial meniscus (DMM) mouse model of OA was established to assess cartilage morphology, ferroptosis markers, and histological changes after intra-articular injection of treatments.

Results: MXene-loading significantly enhanced quercetin's protective effects in IL-1β-induced primary mouse ACs, including improved cell viability and proliferation, reduced apoptosis, alleviated oxidative stress, and suppression of ferroptosis. In OA mice, MXene–quercetin treatment more effectively preserved cartilage integrity and inhibited ferroptosis compared with free quercetin.

Conclusion: These findings suggest that MXene can serve as a biocompatible carrier to improve quercetin delivery in osteoarthritis models, supporting its potential for further preclinical evaluation.

Keywords: osteoarthritis, quercetin, MXene, chondroprotective, ferroptosis

Introduction

Osteoarthritis (OA), a complex, multifactorial chronic degenerative joint disease affecting the entire joint, poses a significant healthcare burden due to its high prevalence and impact on patients' quality of life. It is characterized not only by the degradation of articular cartilage and alterations in subchondral bone but also involves pathological changes in the synovial membrane, menisci, tendons, ligaments, and notably the infrapatellar fat pad (IFP), which forms an integrated unit with the synovial membrane. In OA patients, the IFP exhibits inflammation and fibrosis, with reduced volume compared to patients with meniscal tears, underscoring its important role in OA pathophysiology.[1,2] The main risk factors for OA include aging, joint injury, obesity, genetic predisposition, and mechanical overload.[3,4]

Received: 13 May 2025
Accepted: 28 August 2025
Published: 20 September 2025

Current OA treatments mainly focus on symptom relief and do not effectively halt disease progression.[5] Cartilage homeostasis is maintained by a delicate balance between chondrocyte proliferation and death, and disruptions in this balance are associated with OA progression.[6–8] OA pathogenesis involves oxidative stress characterized by accumulation of lipid reactive oxygen species (ROS) and depletion of antioxidants such as glutathione (GSH).[9] Ferroptosis, a form of programmed cell death distinct from apoptosis, necrosis, and autophagy, has recently been implicated in OA development, representing a promising therapeutic target.[10–12]

Quercetin, a natural flavonoid with antioxidant properties, has demonstrated chondroprotective effects by inhibiting chondrocyte apoptosis and ferroptosis in various disease models.[13,14] However, its clinical translation is limited by poor bioavailability and stability.[15] To overcome these challenges, nanomaterials have been increasingly employed as drug delivery vehicles to enhance drug stability and targeted delivery.[16]

MXene, a novel two-dimensional nanomaterial, has attracted extensive attention in biomedical applications due to its superior mechanical, thermal stability, and electrochemical properties. It exhibits excellent biocompatibility, non-toxicity, and low immunogenicity, making it a promising carrier for in vivo drug delivery.[17,18] MXene's high specific surface area enables a high drug loading capacity, and its surface reactive sites facilitate functionalization with biomolecules and polymers for targeted delivery.[19] Importantly, recent studies have begun to explore MXene's applications specifically in cartilage repair, highlighting its potential advantages over generic nanocarriers.[20]

Additionally, hydrogel-based MXene composites have been shown to further enhance cartilage regeneration and repair by providing a conducive microenvironment and sustained drug release.[21] However, to date, few studies have evaluated MXene as a delivery system for quercetin in OA, leaving a scientific gap that this study aims to address. Our work aims to clarify this by investigating the efficacy of quercetin-loaded MXene nanoparticles in alleviating OA through anti-ferroptotic mechanisms, offering potential clinical significance for OA management.

Materials and Methods

Preparation and Evaluation of Quercetin-MXene

To prepare porous MXene, 50 mL of a 10 mg/L MXene Ti_3C_2 nanosheet solution (BKNANO-MEDICAL, Suzhou, China) was combined with an equal volume of 0.05 M anhydrous copper acetate (Aladdin, Shanghai, China). The mixture was magnetically stirred at 25 °C for 30 minutes, then centrifuged and washed three times at 3,500–7,000 rpm to completely remove Cu^{2+} ions. The resulting precipitate was treated with a diluted hydrofluoric acid solution for 10 minutes, centrifuged at 8,000 rpm, and washed with H_2O until the pH reached approximately 6, yielding porous MXene nanosheets. These porous MXene nanosheets (10 mg) were then combined with PEG-NH_2 (20 mg, MW 2000, Shanghai Macklin Biochemical Co., Ltd., China), dispersed in water, and subjected to ultrasonic treatment for 30 minutes. The solution was then centrifuged, the supernatant discarded, and the nanomaterials were dried for further use. To prepare porous MXene loaded with quercetin, a 10 mg/mL porous MXene solution was first prepared by dispersing the material in MilliQ water with magnetic stirring at room temperature. A 5 mg/mL DMSO solution of quercetin (Q4951, Sigma-Aldrich, St. Louis, MO, USA) was then added dropwise to the porous MXene solution (at a ratio of 10:1) under continuous stirring at 600 rpm for 20 minutes. The mixture was subsequently sonicated for 5 minutes to ensure dispersion and left stirring overnight. Finally, the solution was centrifuged at 11,000 rpm for 10 minutes and freeze-dried for further experimentation. The quercetin-MXene samples were characterized using transmission electron microscopy (TEM; Hitachi Regulus, Tokyo, Japan), scanning electron microscopy (SEM; Hitachi HF5000, Japan), and ultraviolet-visible spectroscopy (UV-Vis; N45 spectrophotometer, Yidanfenxi, Shanghai, China). To assess the stability of quercetin-MXene, the material was dispersed in an aqueous solution, PBS buffer, and DMEM complete medium, and dynamic light scattering (DLS; Malvern Zetasizer Nano ZS, UK) was employed to monitor changes in the hydrodynamic size for 7 days. To test the release status of quercetin, quercetin-MXene was placed in a phosphate buffer solution containing 10% bovine serum albumin (BSA), and the absorbance of the solution was measured at 374 nm using UV spectrophotometry at intervals of 0, 0.5, 1, 3, 5, 7, 9, 11, 13, and 15 days. A standard curve was generated from a quercetin standard to calculate the quercetin concentration in solution over time.

Cell Culture

The primary ACs were obtained from Pricella Biotechnology (Wuhan, China) and cultured with a specialized medium (CM-M092, Pricella Biotechnology) in an incubator at 37 °C with 5% CO_2. For the IL-1β treatment, ACs were seeded into 96-well plates at a density of 8,000 cells per well and allowed to adhere for 6 hours. Following this, the cells were exposed to varying concentrations of murine IL-1β (SRP8033, Sigma-Aldrich, USA) for a duration of 24 hours to induce OA. The IL-1β concentration for OA induction (10 ng/mL) was selected based on previous literature.[22] Drug treatments included quercetin (0–100 μM) or quercetin-MXene at equivalent quercetin doses.

CCK-8 Assay

To assess cell viability, a CCK-8 assay was conducted using a kit obtained from Beyotime Biotechnology (C0037, China). For the IL-1β treatment, ACs were seeded into 96-well plates at a density of 8,000 cells per well and allowed to adhere for 6 hours. Following this, the cells were exposed to IL-1β for 24 hours. Afterward, 10 μL of the CCK-8 working solution was added to each well and incubated at 37 °C for 2 hours. The optical density (OD) at 450 nm (OD_{450}) was then measured using a microplate reader (A51119500C, Thermo Fisher Scientific, USA).

MTT Assay

The MTT assay was carried out using a detection kit (40201ES72, Yeasen, China) according to the manufacturer's instructions. Briefly, ACs were seeded in 96-well plates at a density of 8,000 cells per well. After 6 hours, the cells were treated with different concentrations of quercetin for 24 hours. Subsequently, 10 μL of MTT working solution (5 mg/mL) was added to each well, and the plates were incubated at 37 °C for an additional 2 hours. After incubation, 150 μL of DMSO was added to dissolve the formazan crystals, and the mixture was agitated for 10 minutes at 37 °C on an oscillator at 300 rpm. The OD_{490} was then measured using a microplate reader.

7-Aminoactinomycin D (7-AAD) Staining

7-Aminoactinomycin D (7-AAD) staining was used to assess cell membrane integrity and viability. ACs were seeded into 6-well plates at a density of 1.2×10^6 cells per well and incubated for 6 hours. The cells were then treated with the specified chemicals or PBS for 24 hours. Following treatment, the cells were washed with PBS, digested with trypsin, centrifuged, and fixed with ethanol overnight at −20 °C. The cells were subsequently washed again, resuspended in PBS, and incubated with 100 μg/mL RNase A in PBS containing 0.2% Triton X-100 for 30 minutes at 37 °C. After removing the RNase A, the cells were resuspended in PBS containing 5 μL of 7-AAD solution (ST515, Beyotime Biotechnology) and kept in the dark at room temperature for 10 minutes. Finally, the cells were analyzed using a NovoCyte flow cytometer (1300, Agilent, USA), and the data were processed with the associated software.

Annexin V-FITC/PI Staining

For the apoptosis assay, an Annexin V-FITC/PI apoptosis detection kit (A211-01, Vazyme, China) was utilized as per the manufacturer's guidelines. In brief, ACs were seeded in 6-well plates at a density of 1.2×10^6 cells per well and cultured for 6 hours. The cells were then exposed to the indicated chemicals or PBS for 24 hours. Following treatment, the cells were washed with PBS, digested with trypsin, centrifuged, and resuspended in 100 μL of the binding buffer provided in the kit. Next, 5 μL of Annexin V-FITC and 5 μL of PI solution were mixed with the cell suspension and incubated in the dark at room temperature for 10 minutes. After this incubation, 400 μL of binding buffer was added, and the cells were analyzed by flow cytometry.

Western Blot

Protein extraction from cells or tissues was performed using RIPA lysis buffer (Beyotime Biotechnology) supplemented with protease inhibitors, following the manufacturer's protocol. The samples were combined with a loading buffer and denatured for 5 minutes at 95 °C. Proteins were then separated by electrophoresis using prestained protein ladder (G2086-250UL) and transferred onto PVDF membranes, which were blocked using a solution of nonfat dry milk

(Beyotime Biotechnology). The membranes were incubated with primary antibodies overnight at 4 °C. After washing three times with Tris-buffered saline containing 0.1% Tween-20 (TBST), the membranes were treated with blocking solution containing horseradish peroxidase (HRP)-conjugated goat anti-rabbit IgG (#SA00001-2, Proteintech, 1:10,000, China) or HRP-conjugated goat anti-mouse IgG (#SA00001-1, Proteintech, 1:10,000) for 2 hours at room temperature. Following three additional washes with TBST, the membranes were incubated with enhanced chemiluminescence (ECL) reagent (Beyotime Biotechnology) for signal detection. In this study, X-ray film was used as the standard method for chemiluminescent detection, which has been systematically optimized in our laboratory. After incubation with HRP-conjugated secondary antibodies, protein signals were detected using ECL substrate (Beyotime Biotechnology). The chemiluminescent signals were captured by exposure to X-ray film (Kodak, R400) for 3 to 5 seconds. Protein levels were normalized to an internal control using Image J software (National Institutes of Health, USA). A list of primary antibodies used can be found in Table 1.

Transwell Assay

ACs were plated into 6-well plates at a density of 1.2×10^6 cells per well and allowed to adhere for 6 hours. The cells were then treated with the specified chemicals or PBS for 24 hours. After treatment, the cells were washed with PBS, digested with trypsin, centrifuged, resuspended, and transferred to 24-well plates containing 8 μm Transwell chambers (3422, Corning, USA) at a density of 80,000 cells per well. For invasion assays, 100 μL of Matrigel (1:5 dilution, 356235, BD, USA) was added to each chamber, and the plates were incubated at 37 °C for 2 hours. Following this, 200 μL of cell suspension was added to the upper chamber, while 700 μL of complete medium was placed in the lower chamber. After 24 hours of culture, the cells were fixed using 4% paraformaldehyde (PFA, P0099, Beyotime Biotechnology) for 30 minutes at room temperature and then stained with 0.05% crystal violet (C0121, Beyotime Biotechnology) for 5 minutes. The results were examined and photographed using an OLYMPUS inverted microscope (Japan), and image analysis was conducted using ImageJ for quantification. For migration assays, the same procedures were followed, except that Matrigel was omitted.

Tracing of Carboxyfluorescein Succinimidyl Ester (CFSE)-Labeled Quercetin

The CFSE dye (40714ES76, Yeasen, China) was mixed with quercetin-MXene at a ratio of 1:1000 and incubated for 2 hours at 37 °C. This mixture was then applied to the cells for either 24 or 48 hours. Following incubation, the cells were washed with culture medium, counterstained with DAPI, mounted, and visualized using an LSM 900 confocal microscope (Zeiss, Germany).

Table 1 Primary Antibody Information

Target	Species	Manufacturer	Catalog#	Dilution
NRF2	Mouse	Proteintech	80593-1-RR	1:500
GPX4	Mouse	Proteintech	67763-1-Ig	1:500
ACSL4	Rabbit	Proteintech	22401-1-AP	1:2000
FTH1	Rabbit	Proteintech	11682-1-AP	1:1000
COX2	Rabbit	Proteintech	12375-1-AP	1:500
β-actin	Rabbit	Proteintech	20536-1-AP	1:1000

Abbreviations: NRF2, Nuclear factor erythroid 2–related factor 2; GPX4, Glutathione peroxidase 4; ACSL4, Acyl-CoA synthetase long-chain family member 4; FTH1, Ferritin heavy chain 1; COX2, Cyclooxygenase-2; β-actin, Beta-actin (loading control).

2′,7′-Dichlorodihydrofluorescein Diacetate (DCF-DA)

The 2′,7′-Dichlorodihydrofluorescein diacetate (DCF-DA) assay kit (50101ES01, Yeasen) was utilized to detect ROS. Briefly, ACs were plated into 6-well plates at a density of 1.2×10^6 cells per well and incubated for 6 hours. The cells were then treated with the indicated chemicals or PBS for 24 hours. Following treatment, the cells were washed with PBS, digested with trypsin, centrifuged, and resuspended in culture medium at a density of 3×10^6 cells/mL. The cells were stained with 10 μM DCF-DA probe at 37 °C for 20 minutes in the dark, with intermittent inversion. Finally, the cells were pelleted, washed with culture medium, and analyzed by flow cytometry.

Measurement of Malondialdehyde (MDA), Reduced Glutathione (GSH), Oxidized Glutathione Disulfide (GSSG), and Fe^{2+} Levels

MDA levels were measured using a lipid peroxidation assay kit (BC0020, Solarbio, China). ACs subjected to the indicated treatments were lysed with the provided extraction buffer, followed by sonication and centrifugation at 8,000 × g for 10 minutes to collect the supernatant. The supernatants were then incubated with MDA detection working solutions. The relative MDA content was calculated based on OD_{450}, OD_{532}, and OD_{600} values, as well as a standard curve, with normalization to the final protein concentration. GSH and GSSG levels were quantified using a GSH/GSSG assay kit (S0053, Beyotime Biotechnology) according to the manufacturer's guidelines. The levels of Fe^{2+} were measured using an Iron Microplate Assay Kit (E-BC-K881-M, Elabscience, China) following the user manual.

TEM

For TEM sample preparation, ACs subjected to the indicated treatments were digested, pelleted, and fixed with a designated fixative for 30 minutes in the dark. The subsequent analysis was conducted by Pinuofei Biological Technology (China) using an HT-7700 electron microscope (Hitachi, Japan).

Construction of the OA Mouse Model

C57BL/6 mice (male, 7-weeks old) were obtained from Beijing Weitonglihua Experimental Animal Technology (China). The mice were housed under a 12-hour light/dark cycle at 22 ± 1°C with 50–60% humidity and had ad libitum access to food and water. Seven-week-old male C57BL/6 mice were randomly divided into five groups (n = 8 per group, with an additional 2 in the model group to confirm successful model construction). After a one-week acclimation period, the mice were assigned to experimental groups. The sham operation group received an intraperitoneal injection of pentobarbital (35 mg/kg) above the right knee joint for joint cavity anesthesia only. The remaining four groups underwent destabilization of the medial meniscus (DMM) surgery, where the medial meniscus ligament was severed to impair meniscal stability. H&E staining confirmed successful model establishment in two mice from the model group. One week post-surgery, the sham and DMM groups received intra-articular injections of saline, while the DMM + drug groups received different drug treatments via intra-articular injection: quercetin (250 μg/kg) once daily for three days and quercetin-MXene or MXene (250 μg/kg) once daily for three days. The dosage rationale for quercetin (250 μg/kg) was based on prior OA studies.[23] Randomization was performed using a random number table, and histopathology scoring was conducted by two independent blinded investigators. Following the treatment period, all mice were euthanized by intraperitoneal injection of an overdose of sodium pentobarbital (350 mg/kg). The articular tissues were dissected and harvested for histological and Western blot analyses. All surgical procedures and perioperative handling were conducted in accordance with protocols (No. AEWC-NBU20240308) approved by the Animal Ethics and Welfare Committee of Ningbo University and following the guidelines for the care and use of laboratory animals as outlined by the National Institutes of Health (NIH) Guide for the Care and Use of Laboratory Animals.

Hematoxylin and Eosin (H&E) and Toluidine Blue Staining

H&E and toluidine blue staining were performed on rehydrated paraffin sections using a kit from Beyotime Biotechnology (C0105S) and a kit from Sangon Biotech (E670105-0100, China), following the manufacturer's instructions.

Statistical Analysis

Statistical analyses and data visualization were performed using Prism (v8, GraphPad, USA). Data are expressed as mean ± standard deviation (SD), with a significance level set at $P < 0.05$. All experiments were conducted independently at least three times, with the MTT and CCK-8 assays including technical triplicates. Normality of data was assessed by the Shapiro–Wilk test. Parametric data were analyzed by one-way ANOVA with Tukey's post hoc test, and non-parametric data by Kruskal–Wallis test with Dunn's post hoc test. Power analysis indicated that n = 8 per group provided >80% power ($\alpha = 0.05$, effect size = 1.5).

Results

Characterization of Quercetin-MXene

To characterize the physical features of quercetin-MXene nanoparticles, we first examined their size and morphology using SEM and TEM. The results revealed that quercetin-MXene has a relatively smooth surface with numerous tiny pores (Figure 1A and B). UV-Vis showed typical absorbance peaks for organic nanomaterials, ranging from 200 to 400 nm (Figure 1C). DLS analysis indicated a consistent hydrodynamic size of approximately 200 nm for quercetin-MXene across all tested solutions over a 7-day period (Figure 1D). Furthermore, UV spectrophotometry demonstrated a steady release of quercetin from quercetin-MXene for at least 15 days (Figure 1E). These findings suggest that MXene is a reliable and stable carrier for quercetin.

Quercetin-MXene Outperforms Quercetin in Improving the Survival and Viability of IL-1β-Induced Chondrocytes

To evaluate the impact of MXene-loading on the effects of quercetin in OA, we first established an OA cellular model by treating mouse ACs with various concentrations of IL-1β, which is widely used for establishing OA models. We found that treatment with 150 ng/mL of IL-1β for 24 hours significantly reduced chondrocyte viability, as shown by CCK-8 assay results (Figure 2A). Additionally, this treatment substantially increased the levels of MDA and Fe^{2+} in ACs (Figures 2B and C), indicating upregulated oxidative stress. We then optimized the concentration of quercetin to ensure it

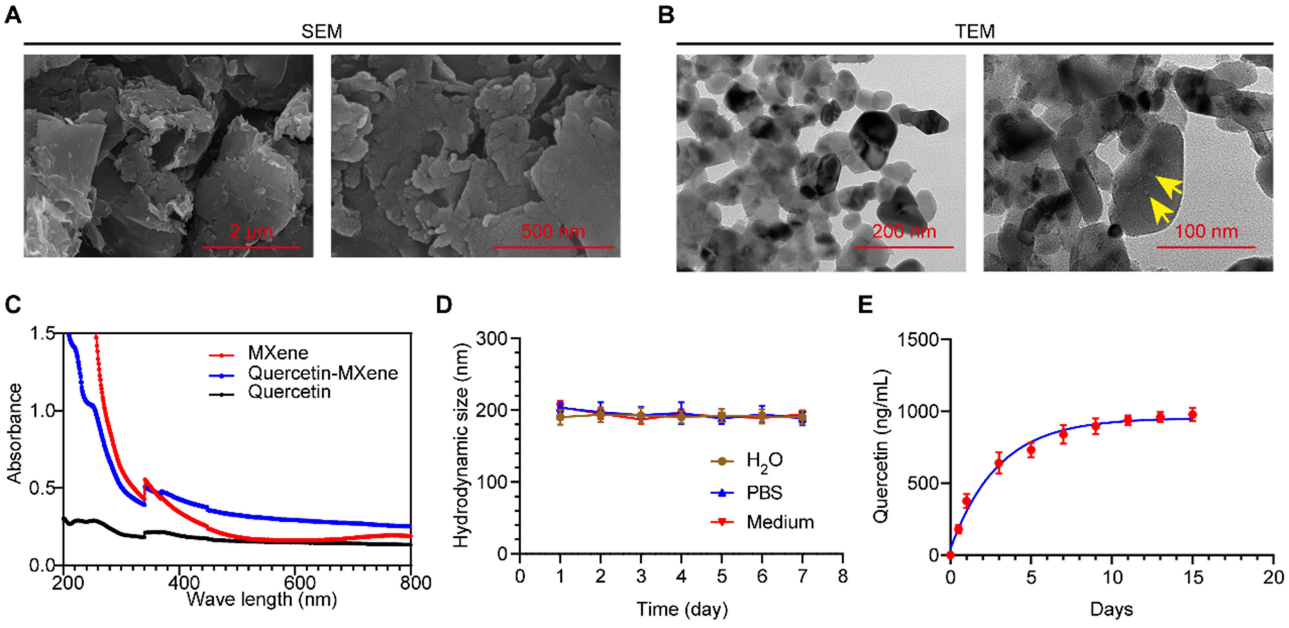

Figure 1 Characterization of Quercetin-MXene (**A** and **B**) SEM (**A**) and TEM (**B**) images showing the morphology and structure of quercetin-MXene. Yellow arrows highlight tiny pore structures within the particles. (**C**) UV-spectroscopy data indicating absorbance wavenumber peaks for quercetin, quercetin-MXene, and MXene. (**D**) DLS data depicting the hydrodynamic size of quercetin-MXene in H_2O, PBS, and culture medium. (**E**) UV spectrophotometry results depicting the concentration of quercetin released from quercetin-MXene over a 15-day period.

was non-cytotoxic to ACs. MTT assay data showed that 200 nM quercetin impaired AC viability (Figure 2D), so we selected 100 nM quercetin for subsequent experiments and MXene-loading. We further labeled quercetin-MXene with CFSE and cultured it with ACs. After 24 or 48 hours, we observed that ACs successfully absorbed the quercetin (Figure 2E).

We then examined the cell cycle of ACs treated with IL-1β in the presence of quercetin, MXene, or quercetin-MXene. The 7-AAD assay results indicated that IL-1β caused more ACs to arrest in the G_0/G_1 phase, with fewer cells entering the S phase, compared to the mock group, which is treated with an equal amount of PBS used to dilute IL-1β. MXene alone had minimal impact on the cell cycle of IL-1β-exposed ACs. Both quercetin and quercetin-MXene promoted cell cycle progression in IL-1β-treated ACs, with quercetin-MXene demonstrating greater efficiency (Figures 3A and B). Annexin V/PI staining results further showed that MXene alone had no discernible anti-apoptotic effect in IL-1β-treated ACs, while quercetin-MXene exhibited a stronger anti-apoptotic effect than quercetin alone (Figures 3C and D). Consistently, quercetin-MXene outperformed quercetin in promoting the viability of IL-1β-treated ACs, as shown by MTT assay results (Figure 3E). Additionally, the impaired migration and invasion of ACs induced by IL-1β were improved by both quercetin and quercetin-MXene, with quercetin-MXene displaying superior efficacy, while MXene alone showed no such effect (Figures 4A–D). These findings suggest that MXene-loading enhances the effect of quercetin in promoting the survival and viability of IL-1β-treated ACs.

Quercetin-MXene Exhibits a Stronger Anti-Ferroptotic Effect in IL-1β-Induced ACs

Given the essential role of ferroptosis in OA, we next explored the effect of MXene-loading on the anti-ferroptotic function of quercetin in IL-1β-treated ACs. We initially measured the levels of MDA, GSH, GSSG, Fe^{2+}, and ROS in these ACs. Results showed that the elevated levels of MDA, GSSG, Fe^{2+}, and ROS, along with the downregulated GSH levels induced

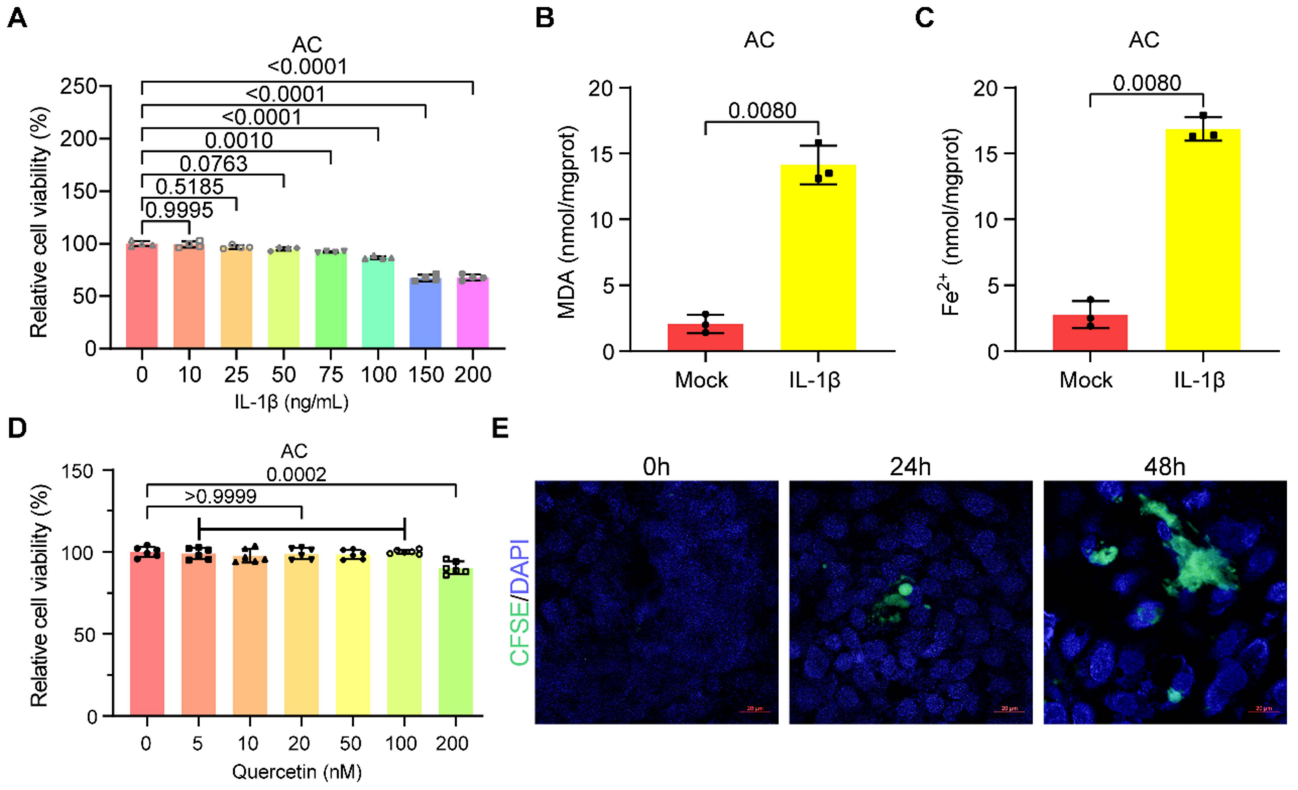

Figure 2 Optimization of IL-1β and Quercetin Dosages in ACs. (**A**) CCK-8 assay results showing the viability of ACs exposed to various concentrations of IL-1β for 24 hours. One-way ANOVA followed by Tukey's multiple comparisons test was used to calculate the P-values. (**B** and **C**) Plots showing the MDA (**B**) and Fe^{2+} (**C**) levels in ACs treated with PBS (Mock) or 150 ng/mL IL-1β for 24 hours. Unpaired two-tailed Student's *t*-test was employed. (**D**) MTT assay results indicating the viability of ACs treated with the specified concentrations of quercetin. One-way ANOVA followed by Tukey's multiple comparisons test was used to calculate the P-values. (**E**) Fluorescence images showing the absorption of CFSE-labeled quercetin by ACs after 24 and 48 hours of culture.

https://doi.org/10.2147/IJN.S540035

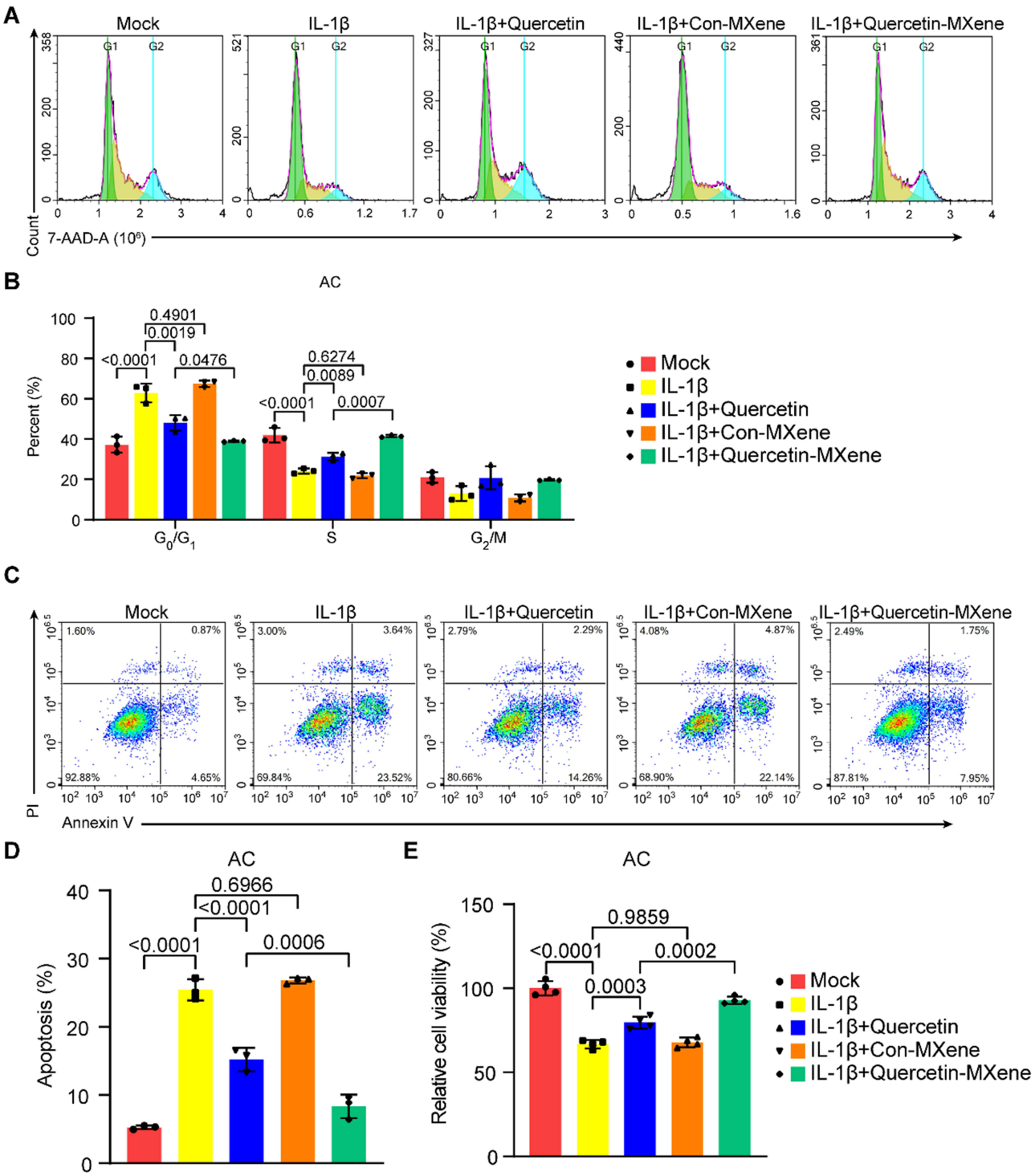

Figure 3 MXene-loading enhances the anti-apoptotic and pro-viability effects of quercetin in ACs treated with IL-1β. (**A**) 7-AAD assay results showing the cell cycle status of ACs under the indicated treatments. (**B**) Quantification of 7-AAD assay data. One-way ANOVA followed by Tukey's multiple comparisons test was used to calculate the P-values. (**C**) Annexin V/PI staining results illustrating apoptosis levels in ACs under the indicated treatments. (**D**) Quantification of Annexin V/PI staining data. One-way ANOVA followed by Tukey's multiple comparisons test was used to calculate the P-values. (**E**) MTT assay results demonstrating the viability of ACs under the indicated treatments. One-way ANOVA followed by Tukey's multiple comparisons test was used to calculate the P-values.

by IL-1β, were significantly improved by both quercetin and quercetin-MXene but not by MXene alone, with quercetin-MXene showing superior efficacy (Figures 5A–G). Additionally, both quercetin and quercetin-MXene improved mitochondrial structure, as indicated by TEM data (Figure 5H). TEM images (Figure 5H) revealed that in the Mock group, mitochondria exhibited normal, intact cristae and a clear matrix, presenting a typical healthy mitochondrial ultrastructure.

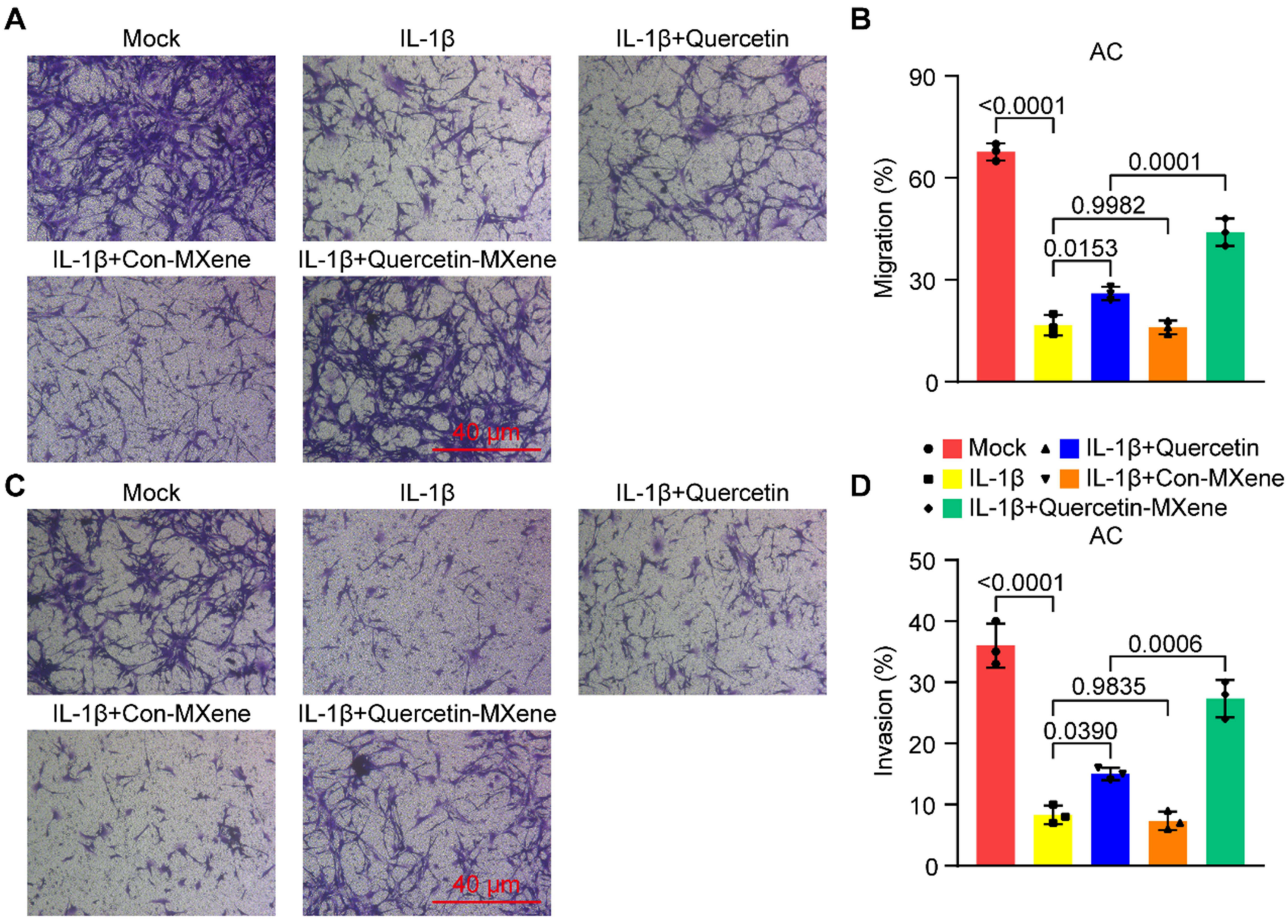

Figure 4 Quercetin-MXene enhances migration and invasion in IL-1β-induced ACs. (**A** and **C**) Transwell assay results showing the migration (**A**) and invasion (**C**) of ACs treated with IL-1β. (**B** and **D**) Quantification of Transwell assay results for migration (**B**) and invasion (**D**) as shown in (**A**) and (**C**). One-way ANOVA followed by Tukey's multiple comparisons test was used to calculate the P-values.

In IL - 1β - treated ACs, mitochondria displayed obvious abnormalities: cristae were disrupted and disorganized, matrices were swollen, and outer membranes showed irregularities, indicative of severe mitochondrial damage induced by IL - 1β. Quercetin treatment partially restored mitochondrial morphology; compared with the IL - 1β group, cristae became more organized, matrix swelling was alleviated to some extent, and the overall mitochondrial structure tended to be more regular. Con - MXene alone had limited improvement on IL - 1β - induced mitochondrial damage, with only slight changes in cristae arrangement and matrix swelling. In contrast, quercetin - MXene treatment led to a more prominent restoration: mitochondria showed well - defined, neatly arranged cristae, compact matrices, and maintained the typical double - membrane structure of mitochondria, indicating a stronger protective effect on mitochondrial morphology against IL - 1β - induced injury.

At the molecular level, MXene-loading enhanced the impact of quercetin on the expression of ferroptosis-related genes, including *NRF2, FTH1, COX2, GPX4*, and *ACSL4*, as evidenced by Western blot results (Figures 5I and J). These findings demonstrate that MXene-loading strengthens the anti-ferroptotic effect of quercetin in IL-1β-induced ACs.

Quercetin-MXene Demonstrates Superior Efficacy Over Quercetin in Repressing Chondrocyte Ferroptosis in an OA Mouse Model

In H&E staining (Figure 6A), the sham group presented articular cartilage with a smooth surface, well - arranged chondrocytes in columns, and intact matrix structure. In contrast, the OA group exhibited obvious cartilage damage: the surface was rough and uneven, chondrocyte arrangement was disordered, and there were defects in the matrix (black arrows), indicating severe structural disruption. MXene alone (OA + Con - MXene group) had no observable

https://doi.org/10.2147/IJN.S540035

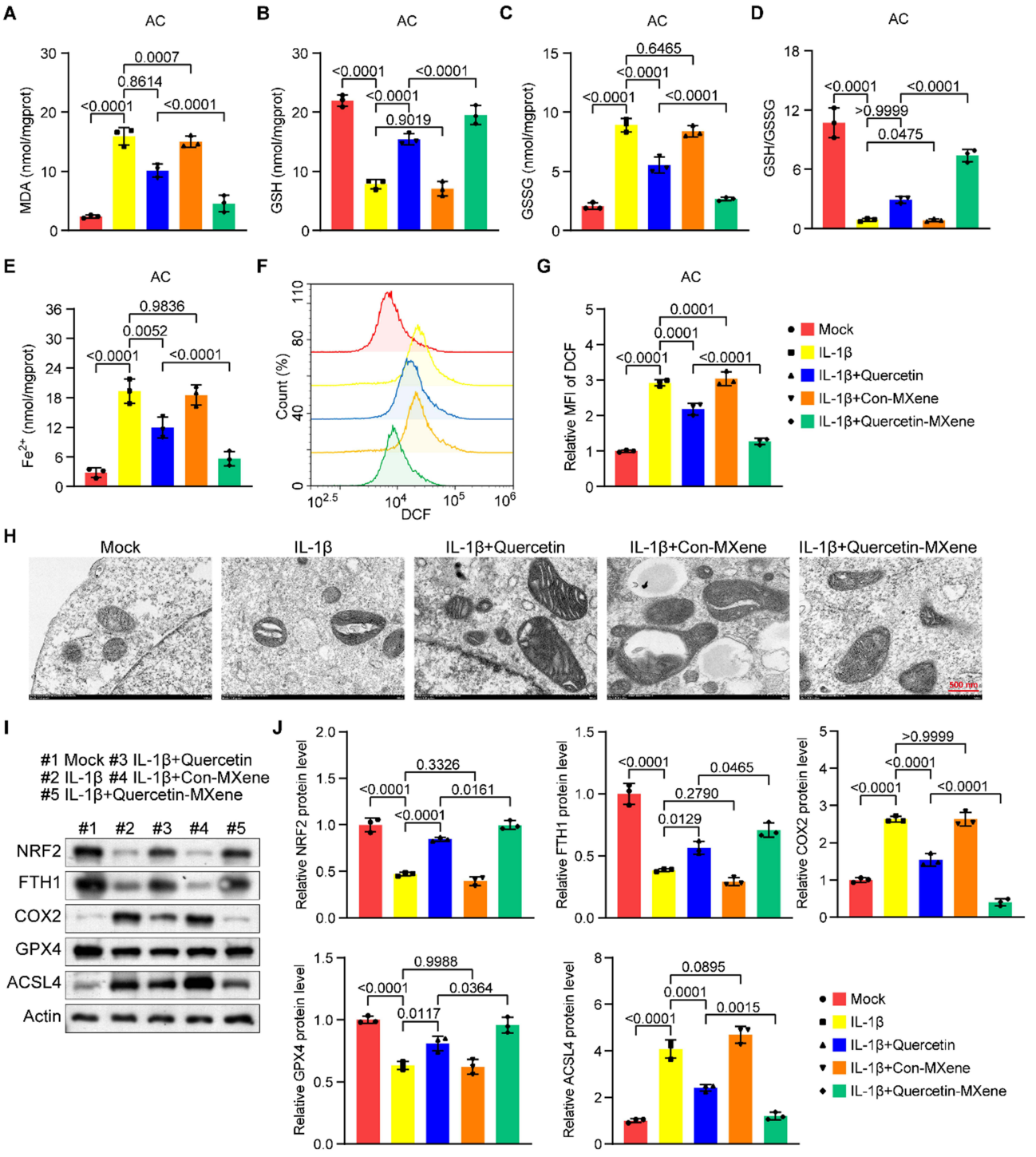

Figure 5 Quercetin-MXene demonstrates a stronger anti-ferroptotic effect than free quercetin in IL-1β-induced ACs. (**A-E**) Plots showing the levels of MDA (**A**), GSH (**B**), GSSG (**C**), GSH/GSSG ratio (**D**), and Fe^{2+} (**E**) in ACs under the indicated treatments. (**F**) DCF-DA staining assay results showing ROS levels in ACs with the indicated treatments. (**H**) TEM images displaying mitochondrial morphology in ACs with the indicated treatments. (**I**) Western blot data showing the expression levels of NRF2, FTH1, COX2, GPX4, and ACSL4 in ACs with the indicated treatments. (**J**) Quantification of the Western blot data. One-way ANOVA followed by Tukey's multiple comparisons test was used to calculate the P-values in all panels.

improvement on the morphology, still showing rough surfaces and disorganized chondrocytes (black arrow). Quercetin treatment (OA + Quercetin group) alleviated cartilage damage to some extent, with the surface becoming relatively smoother and chondrocyte arrangement more regular compared to the OA group. Notably, quercetin - MXene treatment (OA + Quercetin - MXene group) resulted in a more prominent restoration: the articular cartilage surface was smooth,

chondrocytes were neatly arranged in columns, and the matrix structure was well - preserved, demonstrating a stronger protective effect on cartilage morphology.

Toluidine blue staining (Figure 6B) further confirmed these changes. The sham group showed strong and uniform toluidine blue staining, reflecting normal proteoglycan content in the cartilage matrix. The OA group displayed weak and uneven staining, with reduced proteoglycan and damaged matrix (black arrow). Quercetin treatment increased toluidine blue staining intensity and improved uniformity, while quercetin - MXene treatment led to the most significant enhancement of staining, suggesting better retention and restoration of proteoglycans, consistent with the improved cartilage structure observed in H&E staining.

While MXene alone had no observable effect on the morphology of the articular cartilage, both quercetin and quercetin - MXene alleviated cartilage damage (Figures 6A and B). In line with this, quercetin and quercetin - MXene, but not MXene alone, effectively improved the dysregulated levels of MDA, GSH, GSSG, and Fe^{2+} in the articular cartilage tissues of OA mice, with quercetin - MXene showing the best performance (Figure 6C–G). At the molecular level, quercetin - MXene also demonstrated superior efficacy over quercetin in restoring the disrupted expression of *NRF2, FTH1, COX2, GPX4*, and *ACSL4*, as indicated by Western blot results (Figures 6H and I). Together, these data illustrate that MXene - loading enhances the anti - ferroptotic and chondrocyte - protective effects of quercetin on OA chondrocytes in vivo.

Discussion

The medicinal value of quercetin is well-recognized; however, due to its limited absorption efficiency, the efficacy of quercetin and similar natural compounds is often unsatisfactory unless consumed in unrealistic quantities.[24] Consequently, developing novel drug delivery methods has become a major focus in the pharmaceutical industry. Among the emerging delivery carriers, nanomaterials show great promise in enhancing drug delivery efficacy. Supporting this notion, our study demonstrated that quercetin loaded onto MXene (quercetin–MXene) markedly enhanced quercetin's ability to promote viability and survival of OA chondrocytes, both in vitro and in vivo, compared with quercetin alone.[25]

MXene belongs to a family of two-dimensional nanomaterials known for their exceptional electrical conductivity, mechanical strength, and large surface area.[26] Since their discovery, they have attracted considerable interest due to their unique structure and broad range of potential applications.[27] Beyond applications in energy storage, water purification, and electromagnetic interference shielding, MXenes are also being explored for drug delivery due to their biocompatibility.[28] In our study, MXene exhibited minimal cytotoxicity in articular chondrocytes and did not significantly affect cell viability, indicating its biosafety and biocompatibility.[29]

Importantly, our DLS and UV–Vis release data revealed that quercetin–MXene exhibited excellent colloidal stability (~200 nm) in aqueous and physiological media, and sustained quercetin release for up to 15 days. This sustained release, combined with MXene's intrinsic antioxidant capacity reported in previous studies,[30,31] likely contributes to its enhanced chondroprotective effect.

A limitation of our current work is that the specific binding mechanism between quercetin and MXene was not experimentally characterized. Previous reports suggest that polyphenolic compounds such as quercetin can bind to MXene surfaces via hydrogen bonding between phenolic hydroxyl groups and –OH/–O surface terminations, π–π stacking, and Ti–catechol coordination.[32,33] These interactions can influence drug-loading capacity and release kinetics, and future studies should employ spectroscopic and molecular simulation methods to elucidate these mechanisms.

Mechanistically, quercetin–MXene significantly reduced ferroptosis markers (MDA, GSSG, Fe^{2+}, ROS) and restored GSH levels in IL-1β-stimulated chondrocytes, while protecting mitochondrial morphology as observed under TEM. Western blot analysis further showed upregulation of NRF2, GPX4, and FTH1, and downregulation of ACSL4 and COX2, indicating potent ferroptosis inhibition.[34] Prior studies have shown that quercetin can activate AMPK/Nrf2/GPX4 or SIRT1/Nrf2/HO-1 pathways to inhibit ferroptosis in OA models,[35,36] and our results suggest that MXene may synergize with quercetin by lowering ROS burden and facilitating Nrf2 pathway activation.

In vivo, quercetin–MXene treatment in the DMM OA mouse model preserved proteoglycan content, maintained cartilage architecture, and modulated ferroptosis-related protein expression more effectively than quercetin alone.[37]

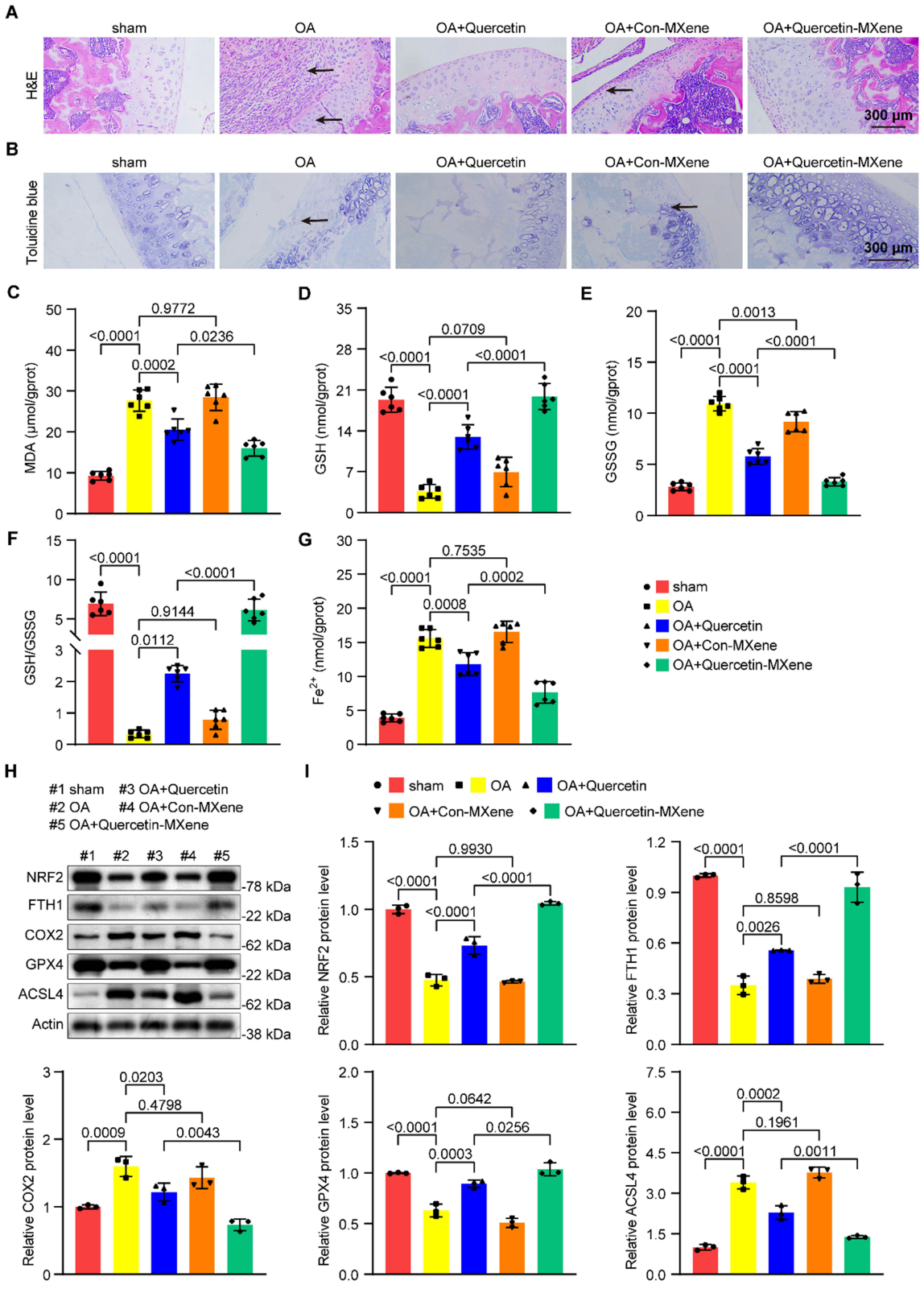

Figure 6 MXene-loading enhances the efficacy of quercetin in reducing OA progression and inhibiting ferroptosis. (**A** and **B**) H&E (**A**) and toluidine blue (**B**) staining showing the morphology of articular cartilage in mice under the indicated treatments. Black arrows indicate damaged cartilage. (**C**–**G**) Plots indicating levels of MDA (**C**), GSH (**D**), GSSG (**E**), GSH/GSSG ratio (**F**), and Fe^{2+} (**G**) in articular cartilage tissues from mice with the indicated treatments. (**H**) Western blot results showing the expression of NRF2, FTH1, COX2, GPX4, and ACSL4 in articular cartilage tissues from mice with the indicated treatments. (**I**) Quantification of Western blot data. One-way ANOVA followed by Tukey's multiple comparisons test was used to calculate the P-values in all panels.

These findings align with previous reports of quercetin-mediated cartilage protection in ACLT and chemically induced OA models via similar antioxidant and anti-ferroptotic mechanisms.[38]

Compared to other delivery strategies, such as lecithin-based nanomicelles,[39,40] pH-responsive ZnO nanoparticles,[41] or quercetin-preconditioned mesenchymal stem cell exosomes,[42] the MXene platform offers the dual advantage of acting as a carrier and contributing intrinsic antioxidative protection, which may uniquely potentiate ferroptosis inhibition in OA.[43]

Nevertheless, our study has several limitations. First, the long-term biosafety, biodistribution, and toxicokinetics of quercetin–MXene remain to be evaluated in large animal models before clinical translation. Second, the binding interactions between quercetin and MXene were not experimentally characterized, as noted above.[32,33] Third, while the IL-1β-induced inflammation model is widely used, it does not fully capture OA's complex inflammatory environment. Macrophage-conditioned medium, such as from differentiated U937 cells,[43] may better represent the in vivo milieu and should be considered in future studies. Finally, intrinsic patient factors such as genetics, metabolism, and lifestyle, which could influence therapeutic efficacy, were not addressed in our current work.

Conclusion

In conclusion, our findings demonstrate that MXene-loading enhances quercetin's bioavailability, prolongs its release, and synergistically augments its anti-ferroptotic and chondroprotective effects in OA models, offering a promising nanomedicine platform for OA therapy. Further mechanistic and translational studies are warranted to optimize this nano-enabled delivery system for clinical use.

Abbreviations

AC, Articular chondrocyte; BSA, Bovine serum albumin; DLS, Dynamic light scattering; DMM, Destabilization of the medial meniscus; GSH, Glutathione; GSSG, Glutathione disulfide; HRP, Horseradish peroxidase; MDA, Malondialdehyde; OA, Osteoarthritis; OD, Optical density; PFA, Paraformaldehyde; ROS, Reactive oxygen species; SD, Standard deviation; SEM, Scanning electron microscopy; TEM, Transmission electron microscopy; UV-Vis, Ultraviolet-visible spectroscopy.

Data Sharing Statement

The datasets used and/or analyzed during the current study are available from the corresponding author on reasonable request.

Animal Ethics Statement

All animal experiments in this study conformed to the animal welfare guidelines under approved protocols (No. AEWC-NBU20240308) of the Animal Ethics and Welfare Committee of Ningbo University, Ningbo, China.

Acknowledgments

This research was supported by Ningbo Top Medical and Health Research Program (Grant No. 2022020102) and Natural Science Foundation of Ningbo (Grant No. 2022J251).

Disclosure

The authors declare no competing interests in this work.

References

1. Zeng N, Yan ZP, Chen XY, Ni GX. Infrapatellar Fat Pad and Knee Osteoarthritis. *Aging Dis*. 2020;11(5):1317–1328.
2. Yue S, Zhai G, Zhao S, et al. The biphasic role of the infrapatellar fat pad in osteoarthritis. *Biomed Pharmacother*. 2024;179:117364.
3. Batushansky A, Zhu S, Komaravolu RK, South S, Mehta-D'souza P, Griffin TM. Fundamentals of OA. An initiative of Osteoarthritis and Cartilage. Obesity and metabolic factors in OA. *Osteoarthritis Cartilage*. 2022;30(4):501–515.
4. Nedunchezhiyan U, Varughese I, Sun AR, Wu X, Crawford R, Prasadam I. Obesity, Inflammation, and Immune System in Osteoarthritis. *Front Immunol*. 2022;13:907750.

5. Richard MJ, Driban JB, McAlindon TE. Pharmaceutical treatment of osteoarthritis. *Osteoarthritis Cartilage*. 2023;31(4):458–466.
6. Hwang HS, Kim HA. Chondrocyte Apoptosis in the Pathogenesis of Osteoarthritis. *Int J Mol Sci*. 2015;16(11):26035–26054.
7. Housmans BAC, Neefjes M, Surtel DAM, et al. Synovial fluid from end-stage osteoarthritis induces proliferation and fibrosis of articular chondrocytes via MAPK and RhoGTPase signaling. *Osteoarthritis Cartilage*. 2022;30(6):862–874.
8. Sandell LJ, Aigner T. Articular cartilage and changes in arthritis. An introduction: cell biology of osteoarthritis. *Arthritis Res*. 2001;3(2):107–113.
9. Riegger J, Schoppa A, Ruths L, Haffner-Luntzer M, Ignatius A. Oxidative stress as a key modulator of cell fate decision in osteoarthritis and osteoporosis: a narrative review. *Cell Mol Biol Lett*. 2023;28(1):76.
10. Dixon SJ, Lemberg KM, Lamprecht MR, et al. Ferroptosis: an iron-dependent form of nonapoptotic cell death. *Cell*. 2012;149(5):1060–1072.
11. Zhang Y, Hu K, Shang Z, Yang X, Cao L. Ferroptosis: Regulatory mechanisms and potential targets for bone metabolism: A review. *Medicine*. 2024;103(39):e39158.
12. Wang J, Yang J, Fang Y, et al. Vinpocetine protects against osteoarthritis by inhibiting ferroptosis and extracellular matrix degradation via activation of the Nrf2/GPX4 pathway. *Phytomedicine*. 2024;135:156115.
13. Wang Y, Wan R, Peng W, Zhao X, Bai W, Hu C. Quercetin alleviates ferroptosis accompanied by reducing M1 macrophage polarization during neutrophilic airway inflammation. *Eur J Pharmacol*. 2023;938:175407.
14. Wang Y, Quan F, Cao Q, et al. Quercetin alleviates acute kidney injury by inhibiting ferroptosis. *J Adv Res*. 2021;28:231–243.
15. Yan Z, Ding N, Lin S, et al. Polysaccharide Based Self-Driven Tubular Micro/Nanomotors as a Comprehensive Platform for Quercetin Loading and Anti-inflammatory Function. *Biomacromolecules*. 2024;25(10):6840–6854.
16. Zheng S, Tian Y, Ouyang J, Shen Y, Wang X, Luan J. Carbon nanomaterials for drug delivery and tissue engineering. *Front Chem*. 2022;10:990362.
17. Deb VK, Jain U. Ti(3)C(2) (MXene), an advanced carrier system: role in photothermal, photoacoustic, enhanced drugs delivery and biological activity in cancer therapy. *Drug Deliv Transl Res*. 2024;14(11):3009–3031.
18. Zhao H, Wang T, Fang X, et al. 2D MXene Nanosheets with ROS Scavenging Ability Effectively Delay Osteoarthritis Progression. *Nanomaterials*. 2024;14(19).
19. Mohajer F, Ziarani GM, Badiei A, Iravani S, Varma RS. Advanced MXene-Based Micro- and Nanosystems for Targeted Drug Delivery in Cancer Therapy. *Micromachines*. 2022;13(10).
20. Kang MS, Jang HJ, Jo HJ, Raja IS, Han DW. MXene and Xene: promising frontier beyond graphene in tissue engineering and regenerative medicine. *Nanoscale Horiz*. 2023;9(1):93–117.
21. Wang H, Zhao Z, Wang Z, et al. Near-infrared Mo(2)Ti(2)C(3) MXene gelatin-chitosan hydrogels with antioxidative, anti-inflammation activity for osteoarthritis treatment. *Int J Biol Macromol*. 2025;307(Pt 3):141979.
22. Sun W, Yue J, Cui Y, et al. Wedelolactone alleviates inflammation and cartilage degeneration by suppressing the NF-kappaB signaling pathway in osteoarthritis. *Int Immunopharmacol*. 2024;143(Pt 1):113359.
23. Yamaura K, Nelson AL, Nishimura H, et al. Therapeutic potential of senolytic agent quercetin in osteoarthritis: A systematic review and meta-analysis of preclinical studies. *Ageing Res Rev*. 2023;90:101989.
24. Alizadeh SR, Ebrahimzadeh MA. Quercetin derivatives: Drug design, development, and biological activities, a review. *Eur J Med Chem*. 2022;229:114068.
25. Hu Y, Gui Z, Zhou Y, Xia L, Lin K, Xu Y. Quercetin alleviates rat osteoarthritis by inhibiting inflammation and apoptosis of chondrocytes, modulating synovial macrophages polarization to M2 macrophages. *Free Radic Biol Med*. 2019;145:146–160.
26. Guo Y, Zhou X, Wang D, Xu X, Xu Q. Nanomechanical Properties of Ti(3)C(2) Mxene. *Langmuir*. 2019;35(45):14481–14485.
27. Soleymaniha M, Shahbazi MA, Rafieerad AR, Maleki A, Amiri A. Promoting Role of MXene Nanosheets in Biomedical Sciences: Therapeutic and Biosensing Innovations. *Adv Healthc Mater*. 2019;8(1):e1801137.
28. Huang H, Jiang R, Feng Y, et al. Recent development and prospects of surface modification and biomedical applications of MXenes. *Nanoscale*. 2020;12(3):1325–1338.
29. Huang R, Chen X, Dong Y, et al. MXene Composite Nanofibers for Cell Culture and Tissue Engineering. *ACS Appl Bio Mater*. 2020;3(4):2125–2131.
30. Li Y, Fu R, Duan Z, Zhu C, Fan D. Artificial Nonenzymatic Antioxidant MXene Nanosheet-Anchored Injectable Hydrogel as a Mild Photothermal-Controlled Oxygen Release Platform for Diabetic Wound Healing. *ACS Nano*. 2022;16(5):7486–7502.
31. Zhao X, Wang LY, Li JM, et al. Redox-Mediated Artificial Non-Enzymatic Antioxidant MXene Nanoplatforms for Acute Kidney Injury Alleviation. *Adv Sci*. 2021;8(18):e2101498.
32. Yao S, Jiang J, He Q, et al. Polyphenolic nanodots loaded multi-layer MXene for strong, tough and rapidly biodegradable polyvinyl alcohol/starch nanocomposites with self-healing ability and improved aging resistance. *Carbohydr Polym*. 2025;368(Pt 1):124104.
33. Meng X, Sun Y, Yu M, Wang Z, Qiu J. Hydrogen-Bonding Crosslinking MXene to Highly Robust and Ultralight Aerogels for Strengthening Lithium Metal Anode. *Small Sci*. 2021;1(9):2100021.
34. Huo L, Liu C, Yuan Y, Liu X, Cao Q. Pharmacological inhibition of ferroptosis as a therapeutic target for sepsis-associated organ damage. *Eur J Med Chem*. 2023;257:115438.
35. Dong S, Li X, Xu G, Chen L, Zhao J. Quercetin attenuates the symptoms of osteoarthritis in vitro and in vivo by suppressing ferroptosis via activation of AMPK/Nrf2/Gpx4 signaling. *Mol Med Rep*. 2025;31(3).
36. Sun B, Cai F, Yu L, An R, Wei B, Li M. Quercetin inhibits ferroptosis through the SIRT1/Nrf2/HO-1 signaling pathway and alleviates asthma disease. *Transl Pediatr*. 2024;13(10):1747–1759.
37. Heydari Nasrabadi M, Parsivand M, Mohammadi N, Asghari Moghaddam N. Comparison of Elaeagnus angustifolia L. extract and quercetin on mouse model of knee osteoarthritis. *J Ayurveda Integr Med*. 2022;13(2):100529.
38. Feng K, Chen Z, Pengcheng L, Zhang S, Wang X. Quercetin attenuates oxidative stress-induced apoptosis via SIRT1/AMPK-mediated inhibition of ER stress in rat chondrocytes and prevents the progression of osteoarthritis in a rat model. *J Cell Physiol*. 2019;234(10):18192–18205.
39. Chen LC, Chen YC, Su CY, Hong CS, Ho HO, Sheu MT. Development and characterization of self-assembling lecithin-based mixed polymeric micelles containing quercetin in cancer treatment and an in vivo pharmacokinetic study. *Int J Nanomedicine*. 2016;11:1557–1566.
40. Chen L, Mei L, Feng D, et al. Anhydrous reverse micelle lecithin nanoparticles/PLGA composite microspheres for long-term protein delivery with reduced initial burst. *Colloids Surf B Biointerfaces*. 2018;163:146–154.

41. Zheng C, Wang Y, Phua SZF, Lim WQ, Zhao Y. ZnO-DOX@ZIF-8 Core-Shell Nanoparticles for pH-Responsive Drug Delivery. *ACS Biomater Sci Eng*. 2017;3(10):2223–2229.
42. Lu M, Lou A, Gao J, et al. Quercetin-primed MSC exosomes synergistically attenuate osteoarthritis progression. *J Orthop Surg Res*. 2025;20 (1):373.
43. Liu J, Lu W, Lu X, Zhang L, Dong H, Li Y. Versatile Ti(3)C(2)T (x) MXene for free-radical scavenging. *Nano Res*. 2022;15(3):2558–2566.